AIAA JOURNAL
Vol. 45, No. 10, October 2007

Drag and Heat Transfer Reductions in High-Speed Flows

Afsheen Khamooshi*
The Boeing Company, Seattle, Washington 98101
and
Trent Taylor† and David W. Riggins‡
University of Missouri–Rolla, Rolla, Missouri 65409

DOI: 10.2514/1.29062

A numerical investigation of forward-facing injection from blunt bodies in high-speed flows when coupled with upstream deposition of energy is shown to result in large decreases in overall drag and heat transfer. The problem of upstream-directed injection jet instability is shown to be significantly reduced by the coupling of the two techniques (injection and upstream energy deposition); this allows the jet to penetrate far upstream and stabilize within bounds. When hydrogen is used as the core injectant, the substantial production of water in and near the zone of upstream energy deposition may assist in the efficiency of energy deposition systems. Additionally, by sheathing the hydrogen core with an inert injectant such as nitrogen, the body is cooled and the heat release and resulting zones of water production are removed from the vicinity of the blunt body. Cases are shown in which the overall drag is only 20–30% of the baseline drag, heat transfer is minimal, and jet stabilization and forward penetration is ensured. The impact of turbulence on drag reduction and flow stability (for combined energy deposition and forward-facing injection) is also shown. Although the impact of turbulence on drag reduction results is found to be similar to laminar flow, the turbulence generally increases the stability of the forward-facing injection, delays the partial collapse of the forward-facing jet, and increases the mixing of hydrogen and air. This increase in mixing is shown to result in a more effective energy release associated with the reaction, which is found to further stabilize the injection and results in lower drag. Further studies also indicate that minimum drag and maximum penetration and stability of the jet at the point of maximum penetration can be maintained by active control of the energy deposition location.

Nomenclature

a/b	=	energy deposition aspect ratio
D	=	diameter of bluntbody nose, m
D_j	=	injectant jet diameter, m
$D_{j,\mathrm{H_2}}$	=	hydrogen injectant jet diameter, m
$D_{j,\mathrm{N_2}}$	=	nitrogen injectant jet diameter, m
$D0$	=	baseline drag, N
M_j	=	jet exit Mach number
$M_{j,\mathrm{H_2}}$	=	hydrogen jet exit Mach number
$M_{j,\mathrm{N_2}}$	=	nitrogen jet exit Mach number
P_{tj}	=	jet total pressure, Pa
Q	=	baseline heat transfer rate, W/s
RD	=	drag reduction factor
RQ	=	heat transfer reduction factor
T	=	temperature, K
U	=	x-directional velocity component, m/s
x/D	=	nondimensional distance in the horizontal direction
y/D	=	nondimensional distance in the vertical direction
γ	=	ratio of specific heats
Δ	=	nondimensional shock standoff distance

I. Introduction

THE overall drag force experienced by aerospace vehicles and shapes at hypersonic flight speeds is predominately due to pressurization associated with the formation of strong normal and oblique shock waves in the flow. In addition, aerodynamic drag and high heating associated with locally normal shocks at leading edges are significant issues. Sound engineering design principles for high-speed flight have traditionally tended to recommend a high fineness ratio shape (i.e., structure) to weaken the shock system and specifically reduce resultant pressurization on upstream-facing vehicle surfaces. However, explicit disadvantages of the high fineness ratio shape include structural problems, poor vehicle volumetric efficiency, and increased frictional drag.

Traditionally, energy management onboard an air-breathing hypersonic vehicle has been dominated mainly by propulsive path fuel heat-release issues and structural cooling requirements. At the same time, the external shape and lines of the vehicle have been determined largely by a passive response to the external aerodynamics in terms of reducing drag, generating adequate lift, and assuring adequate mass capture and upstream diffusion for the propulsion system. However, due to the demanding flight characteristics for a hypersonic vehicle (specifically the extremely challenging thrust-to-drag margin), it is necessary to critically reevaluate current concepts of onboard energy management. Specifically, there has been recent interest (and some investment) in the area of enabling technologies involving aeroenergetics (defined here simply as methods and/or technologies for usefully transferring energy into the flowfield upstream or adjacent to a vehicle for the explicit purposes of flowfield or fluid characteristic modification). This general technology includes plasma generation, microwave and laser heating, injection, and other techniques of interest. These technologies, at some level, may now at least begin to allow the conformation of the external flowfield to the vehicle shape, rather than the converse. This issue can be illustrated from the narrow standpoint of the effective balance of propulsive flowpath thrust against the external drag on the vehicle. In considering that balance, the following question arises: Should a certain portion of onboard energy (whether viewed in terms of fuel or other stored/extracted energy sources) be used to decrease the external drag, or should it be used to increase the propulsive thrust? Note that the answer is clear (at least conceptually) if all else is equal; for example, if one unit of

Presented as Paper 0660 at the 44th AIAA Aerospace Sciences Meeting and Exhibit, Reno, NV, 9–12 January 2006; received 28 November 2006; revision received 28 May 2007; accepted for publication 9 July 2007.

*Engineer, High-Speed Aerodynamics. AIAA Member.
†Graduate Research Assistant, Mechanical and Aerospace Engineering. AIAA Student Member.
‡Professor of Aerospace Engineering, Mechanical and Aerospace Engineering. AIAA Senior Member.

onboard and available power can be used to decrease the drag power five units and that same unit of onboard power would have only increased the thrust power by two units, then the use of that one unit of energy should "certainly" be directed toward drag reduction.

Recent investigations have focused on a variety of nonstructural techniques that have been proposed for significantly reducing the drag forces on hypersonic vehicles, as well as for possibly inducing moments without movable surfaces for stability and control purposes. These techniques are often based upon the concept of developing significant flowfield modification upstream of and adjacent to the vehicle or vehicle surface of interest such that the shock wave system associated with the vehicle or surface (whether forebody, nose, or leading edge) is weakened. In effect, the apparent local fineness ratio of the vehicle or shape (the fineness ratio seen by the oncoming flow) is significantly increased. This significant flowfield modification is optimally accomplished with minimal (small) perturbations in the flowfield. Considerable drag reductions (up to 50% of baseline drag) on a reference blunt body have been achieved in previous numerical studies by the use of localized upstream heating (energy deposition). These studies have relied on energizing small zones upstream of the blunt body face; there is then substantial coupling between energized zones and the blunt body such that the blunt body shock is pulled far forward and forms a much weaker oblique shock. There are a number of studies [1–8] which examine both the physics of the energy deposition process and discuss and quantify drag and heat transfer reduction and flowfield modification involving energy deposition or other similar methods.

Studies have also shown the effectiveness of carefully tailored upstream (forward-facing) injection in causing substantial modifications in shock wave structure and, hence substantial reductions in overall drag and heat transfer (even accounting for the adverse impact of the forward-facing jet momentum). In fact, in the case of forward-facing gaseous injection, heat transfer on the blunt body has been found to actually indicate cooling of the body, along with attendant drag reductions of up to 40%. Studies focused on forward injection and forward spike phenomena in high-speed blunt body flows include [9–20].

Although these two techniques (upstream focused energy deposition and forward-facing injection) have subsequently attracted a substantial amount of interest due to the large potential in reducing overall drag (and heat transfer) as well as allowing volumetrically efficient hypersonic shapes, there have been several major problems with their implementation. In the case of upstream energetics, the question arises as to how energy can be deposited into the flow (i.e., what mechanism is to be used). A number of candidates have been proposed, including microwaves. Unfortunately, the absorption of microwave energy into clean air at some preselected zone is somewhat problematic, although efforts are being made in this area due simply to the large benefits of the drag reduction. In addition, heating a zone upstream of the blunt body may lead to a high-temperature stream of air washing over the body itself. The major problem with forward-facing injection is the instability of the jet, which has been observed both experimentally and numerically. This instability is usually manifested in the jet collapsing completely with little or no forward penetration of the injectant. Although there are regimes of jet-to-freestream dynamic pressure for which the jet is somewhat stable at lower flight Mach numbers, the overall technique of using forward-facing jets for drag and heat transfer reduction is viewed unfavorably due to this single issue of jet instability.

This paper describes results of a numerical investigation of an innovation involving these methodologies which has the potential to alleviate their major limitations. Specifically, the baseline configuration of interest is a forward-facing fuel jet (H_2) which is injected upstream of a blunt body (see Fig. 1). The nozzle design for the fuel injector may be such that the fuel jet itself is sheathed in an injected inert gas (here chosen as nitrogen) such that (conceptually) the fuel penetrates well away (upstream) of the blunt body before it can mix with air and begin combustion. The inert gas, in addition to separating the hydrogen jet from the air near the body, also flows back over and insulates the blunt body such that heat transfer to the body surface will be very small. However, well forward of the body, there is localized energy release associated with chemical reaction, which, along with the forward-facing injection itself, modifies the shock wave structure associated with the blunt body. In addition, a zone of energy deposition is located upstream. The flowfield associated with an energized zone by itself has been shown to result in a Mach tunnel which burrows upstream between the energized zone and the body. The dual use of the energized zone and the injection will be shown in this study to entrain the jet upstream and stabilize it within bounds. When correctly configured, the chemical reaction between fuel and air (oxygen) occurs at or near the location of the energized zone itself, thus producing water and other product species which are far more amenable to microwave heating than clean air. Note that this configuration is a *synergistic* combination of five main effects: 1) forward-facing injection of fuel with upstream penetration, 2) heat release associated with chemical reaction well forward of the body, 3) cooling of the body by the sheathing injectant, 4) chemical compositional changes due to the chemical reaction which may enable or assist efficient microwave or radiative heating, and 5) localized microwave (or other) heating.

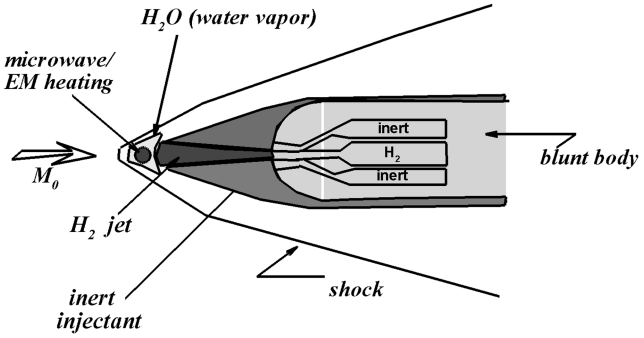

Fig. 1 Schematic of concept involving energy deposition, injection, reaction.

As will be shown subsequently in this paper, a major benefit of the synergistic combination of upstream injection and upstream energization of the flow (i.e., via microwave) is the dramatic increase in jet stabilization and increased forward penetration of the jet; drag reductions for the combination are significantly greater than for the single mechanisms. This and similar concepts may in fact allow for a radical rethinking of both 1) external aerodynamic shape tailoring and resulting propulsion requirements and 2) fuel injector–flow path design for high-speed flight.

The layout of the paper consists of three main sections. The first section summarizes generic configurations examined, provides flow and injection conditions modeled in this study, and provides information regarding the numerical techniques/solvers used, as well as a discussion of the transient/temporal behavior of the flowfields encountered in this investigation. The second section of this paper focuses on results obtained by using a two-dimensional (laminar) Navier–Stokes code named SPARK. Primary interest is in understanding and quantifying physical behavior and performance after jet and flowfield stabilization, i.e., transient effects are not of interest. The third section of the paper provides and analyzes results obtained by using the more sophisticated viscous upwind algorithm for complex flow analysis (VULCAN) computational fluid dynamics (CFD) code (turbulent or laminar Navier–Stokes code with massively parallel computing capability). Comparisons are made between laminar and turbulent flowfields for the given problem of interest with particular emphasis on the drag reduction factor. Time-dependent (transitory) flow visualizations are then presented that examine initial jet/injection/flowfield behavior; this is done to fully understand the potential for active control of the injection/energy deposition for maximum penetration and localization of water production. Finally, an example case using active jet control for maintaining maximum penetration and jet stability is presented.

II. Description of Configurations Studied, CFD Codes, and Grids

In the present study, a two-dimensional hemispherical-nosed blunt body with a 1.5 cm nose diameter is modeled in Mach 10 flight. As discussed in the Introduction, the specific purpose of this study is to investigate the *combined* effects on a blunt body in hypersonic flight of both upstream energy deposition with forward-facing injection. Therefore, a similar blunt body configuration, as used in earlier numerical studies for forward-facing injection alone and energy deposition alone, is modeled here (i.e., see Meyer et al. [14,15] and Taylor et al. [5–7]). Ambient air conditions are calculated based on 30 km (∼100, 000 ft) altitude (1185.5 Pa and 231.24 K). For heat transfer studies, the body surface temperature is held at 500 K, otherwise, the body is treated as adiabatic. Viscous (no slip) conditions are used at the body surface. Drag contributions due to pressure, skin friction, and forward-facing injection are integrated and summed to obtain the total drag associated with the configuration.

Figures 2 and 3 are schematics of two of the injection configurations used in this study. These figures show the side and "frontal" views of the blunt body, which actually represents a two-dimensional wing slab. Forward-facing injection is modeled by setting the values of velocity, pressure, temperature, and species type on the nose of the blunt body (the nodes representing the jet orifice centered on the centerline of the body) to the appropriate values; the injection velocity is in the (negative) x direction. Specifically, Fig. 2 is a schematic for a single injectant configuration without energy deposition, in which a gas (in this study, N_2) is injected from the leading edge of the blunt body. In all cases, unless otherwise indicated, the value of the nondimensional forward-facing jet diameter D/D_j (defined as the blunt body diameter D divided by the forward-facing jet diameter D_j) is kept constant at 63. This value is chosen based on the minimum nondimensional forward-facing jet diameter value used in a previous study by Meyer [14]. Figure 3 is a schematic of a "sheathed" injection configuration, where a jet of H_2 is injected into the incoming flow and is sheathed by N_2 injection. The nondimensional forward-facing hydrogen jet $D/D_{j,H_2}$ is defined as the blunt body diameter D divided by the forward-facing hydrogen jet diameter D_{j,H_2}, whereas the nondimensional forward-facing nitrogen jet $D/D_{j,N_2}$ is defined as the blunt body diameter D divided by the combined diameters of both upper and lower N_2 injections D_{j,N_2}.

Energy deposition volumes (modeled here as rectangular area along the grid lines) at prescribed location(s) within the flowfield are simply modeled via a source term in the energy equation at all nodes within the energized region, such that the phenomenon represents a calculated localized heating (all energy arriving in the molecular translational mode). Figures 4 and 5 are schematics which show the different energy deposition configurations analyzed. Specifically, Fig. 4 illustrates the blunt body with a generic injection capability and a single energy deposition volume upstream. The single energy deposition volume, designated as A, is located on the centerline at a nondimensional distance x/D from the leading edge of the blunt body (note that the volume of energized region is conveniently defined here as volume per meter width, because the problem is two-dimensional). The energy deposition region aspect ratio a/b of the energy deposition volume and its location x/D are varied to study resulting changes in the flowfield/shock modification (including drag and heat transfer reduction) and jet stability. For the case of single-stream nitrogen injection, the overall energy rate added and the energy density are kept constant at 30 kW and $1.5 \cdot 10^7$ kW/m^3, respectively. These values are chosen based on the minimum energy rate and density values used in a previous study by Taylor [6]. Figure 5 shows a schematic of a case with three energy deposition volumes (A, B, and C). In this case, the two secondary energy deposition volumes B and C are located at equal distances off the centerline, $\pm y/D$ (y/D is the nondimensional distance from the center of the secondary energized regions to the centerline of the primary energy deposition volume A), and at equal $x/D_{\text{secondary}}$ distances from the blunt body (but always downstream of A).

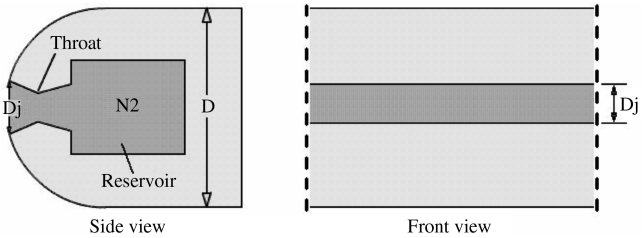

Fig. 2 Blunt body with a single injection configuration.

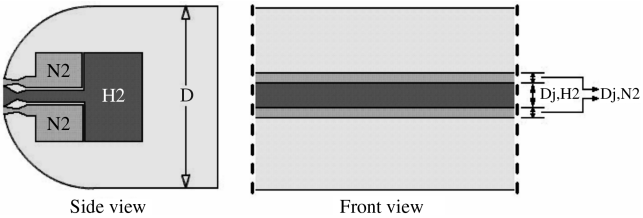

Fig. 3 Blunt body with double injection configuration.

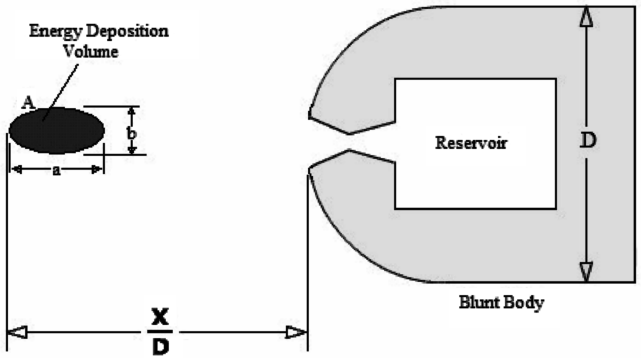

Fig. 4 Blunt body with a single energy deposition volume.

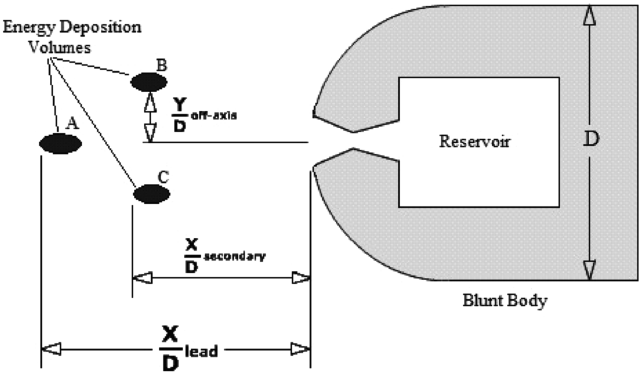

Fig. 5 Blunt body with three energy deposition volumes.

A. SPARK Code

There are two computational fluid dynamics codes used in this study; the SPARK [21] (laminar) two-dimensional Navier–Stokes and the VULCAN [22] computational fluid dynamics solver used for turbulent cases. The first code used in this study is a modified version of the two-dimensional code SPARK, which was originally developed at NASA Langley Research Center for use in studying internal reacting flowfields. Previous works have demonstrated the code's ability to produce reasonable results of the hypersonic blunt body problem [3,5–7,12,14,15]. The code solves the laminar two-dimensional full Navier–Stokes equations by using explicit time-marching. This allows time-dependent studies of unsteady or quasi-steady flowfields and resulting flowfield development. For some

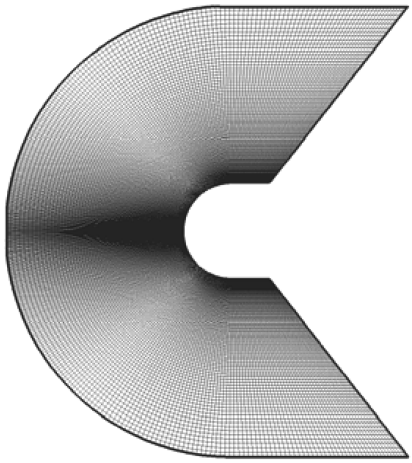

Fig. 6 Grid used for SPARK studies.

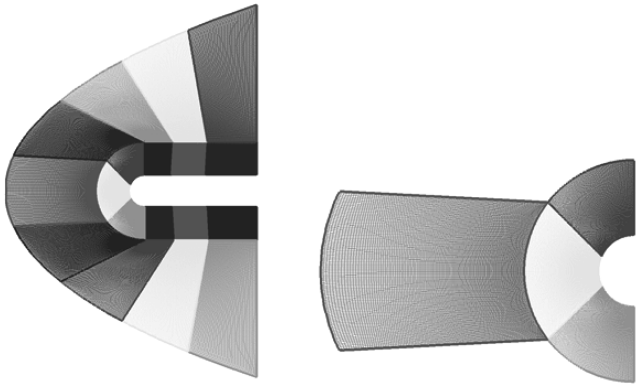

a) **b)**

Fig. 7 Grid used for VULCAN studies: a) full grid, b) subset used for visualization of results.

cases examined in this study, which modeled hydrogen–air chemistry, a seven reaction—seven species finite rate kinetics model for hydrogen–air chemistry [6] is used. These species are as follows: H, H_2, H_2O, OH, N_2, O, and O_2.

1. SPARK Grid/Body Geometry

Figure 6 shows a sample grid used for these case studies using the SPARK code. Although the domain of interest is symmetric about the body centerline, flowfield symmetry is not assumed in this study to allow the possible development of asymmetrical flowfields (especially important in time-accurate and injection studies). The baseline grid shown uses 401×125 grid nodes in a C-grid configuration, meaning the grid uses 401 radial body grid points (starting from the bottom right of the body and counting to the top right corner) and 125 axial grid points (beginning at a body grid point and moving away from the body). The grid is clustered in the path of the forward-facing jet and near the surface of the blunt body.

2. SPARK Grid Convergence

In this investigation, the grid from Meyer's previous study [14] was directly used for preliminary cases. Meyer conducted and presented a detailed analysis of grid convergence for forward-facing injection for a similar configuration as examined here; this analysis is presented in his work and was in terms of overall pressure and skin friction drag and heat transfer and also used the same SPARK code. The grid used in the SPARK portion of the current study (401×125 nodes in the full domain) is in all spatial dimensions finer than Meyer's grid (145×97 nodes in the half-domain); hence, grid convergence for both drag and heat transfer is obtained. Meyer used the body centerline as a symmetry plane, which reduced the usefulness of obtained results from the standpoint of capturing/analyzing jet instability. The current study specifically doubled the grid (incorporating both upper and lower domains around the body) to fully study jet instability and resulting asymmetries in the flowfield. In addition, clustering in the vicinity of the jet orifice is used to capture and resolve the gradients in that flow region.

B. VULCAN Code

The second CFD code used for this study is VULCAN, version 5.0.0, developed at NASA Langley Research Center [22]. All cases shown are run in a time-accurate manner. Both laminar and turbulent solution options are used for this study to determine influence of turbulence on drag reduction and jet stability. The turbulent solutions use a shear stress transport model variant of the Menter two-equation (k–ω) model. The turbulent intensity and reference turbulence viscosity ratio are set to 1 and 10%, respectively. Wall functions are not used, as the primary quantity of interest in this part of the study is the drag due to pressure, which should not be significantly impacted by near-wall phenomena. However, the VULCAN-predicted heat transfer for laminar cases compared very well with SPARK results (which provided grid-converged heat transfer results as noted earlier). The VULCAN model uses triple-interval curve fits for the thermodynamic properties of all species; curve fits are valid from 10–20,000 K.

There are three categories of cases conducted using the VULCAN code: aeroenergetics only with no reaction, aeroenergetics and injection with no reaction, and aeroenergetics and injection with finite rate reaction. An initial comparison case is also constructed to directly compare results between VULCAN and SPARK. This case uses a 500 K constant body surface (wall) temperature. All other cases analyzed using VULCAN use an adiabatic wall condition because the predominant interest in this part of the investigation is to identify the impact of turbulence on drag reduction and injection stability (rather than heat transfer). All cases which result in flowfield modification use the converged baseline (no flowfield modification) blunt body Mach 10 case as the initial (time $= 0$) flowfield condition; this baseline is either laminar or turbulent depending whether the flowfield modification simulation is laminar or turbulent. Chemical species modeling is provided in all cases (no injection, mixing, and reacting) using up to 12 species. These species are as follows: H, HNO, HO_2, H_2, H_2O, N, NO, NO_2, N_2, O, OH, and O_2. For the cases using finite rate reaction, 24 reactions are modeled [22].

1. VULCAN Grid/Body Geometry

The VULCAN code is implemented using an 18 node computer cluster. This requires that the computational domain be separated into 18 discrete blocks of grid. To reduce the size of the output data files for visualization, only data obtained from four grid blocks are used. Figure 7 shows the full 18 block domain used in the solution procedure and the four block domain used for visualization of the obtained results.

Note that the body of revolution for the VULCAN studies is much longer (i.e., continues further downstream) than that studied using SPARK. Furthermore, for the VULCAN cases, the physical domain around the body itself is larger. However, because the bodies used in SPARK and VULCAN have different lengths, only the hemispherical nose sections are examined for the comparison between SPARK and VULCAN results. Each of the 18 grid blocks consist of 101×151 grid points (cells) with 100 cells along the surface of the body and 150 cells emanating radially outward from the body surface. Grid points are clustered at the nose of the body and at the surface of the body (see Fig. 7). All connections between the various grid blocks are point-to-point continuous. The software package GRIDGEN is used to smooth the grid and ensure that lines are normal at the body surface and at block connections.

2. VULCAN Grid Convergence

The grid from Meyer's study [14] using SPARK was also originally examined in the VULCAN studies reported on here. The grid in Fig. 7, however, has a much higher grid density than

Meyer's original grid. VULCAN also has the capability to output the y^+ variation along the surface of the body. Note that a y^+ of approximately 1.0 or smaller is generally considered sufficient for heat transfer and skin friction calculations, whereas the y^+ necessary for pressure convergence (and hence pressure drag) is of course much larger and easier to obtain on a coarse grid. For the turbulent Mach 10 baseline case in VULCAN, the y^+ is found to be 0.4 at the trailing edge of the body, and ranges from 1 to 4.4 on the nose of the body. The cases with energy deposition (no injection) have y^+ values ranging from 1 to 3, whereas cases with energetics and injection (with or without reaction) have values ranging from 0.5 to 2.5 on the nose of the body. Note that the primary quantity of interest in the (turbulent) VULCAN studies is pressure-dominated drag reduction rather than wall heat transfer. Nevertheless, the heat transfer reduction, as well as drag reduction, are almost identical on a representative case between SPARK (extensively examined for grid-converged quantities of interest) and VULCAN.

III. SPARK Results: Laminar Flows

In this work, a drag reduction factor is designated as *RD*, and is defined as the modified drag value divided by the baseline (no flowfield modification or injection) drag, i.e., lower values of *RD* indicate lower overall drag. Overall drag force on a given configuration includes pressure drag, skin friction drag, and the effective drag due to any reverse-thrust (upstream-directed) injection. Similarly, the heat transfer reduction factor is designated as *RQ*, defined as the flowfield modified heat transfer over the baseline (no flowfield modification or injection) heat transfer, i.e., lower values of *RQ* indicate lower overall heat transfer.

The nature of the flowfields examined in this study (particularly with forward-facing injection) is generally quasi steady (i.e., overall drag and heat transfer on the blunt body reach an asymptotic value but manifest small oscillations around this value). There is an initial period when the injection plume penetrates far upstream (corresponding to a maximum drag reduction, etc.) followed by a partial asymmetric collapse of the jet from that transient maximum penetration situation. The jet and shock structure (and associated drag and heat transfer reductions) then tend to stabilize within physical bounds, which are described in later sections, but generally continue to oscillate. (Note that without energy deposition, the injection simply flaps back over the surface of the body with little or no penetration for almost all cases, a fact that has precluded much interest in the technique of forward-facing injection for any application.) However, all flow contour results presented in this paper are simply snapshots at selected times (i.e., at discrete iterations) and for SPARK are only shown once the quasi-steady behavior of the flowfield has been reached (as measured by stabilization of jet within bounds and overall pressure and heat transfer convergence).

Therefore, all results from SPARK are obtained by running an additional 330,000–1,000,000 iterations beyond the time that the flowfield is completely developed and has reached a quasi-steady state as measured by overall pressure and heat transfer. Data are then obtained at 30,000 iteration increments during this process for time averaging of the overall drag, heat transfer, and stability/instability information discussed later (i.e., the data relating to the initial period when the injection plume penetrates far upstream of the body are not used for time averaging). For a representative SPARK time/iteration distribution of overall drag on a flowfield modification case, see Fig. 8. All analysis of the flowfields using the SPARK code (including a detailed statistical analysis of the temporal and spatial behavior [23] not presented here) are done after the initial transients due to flowfield initialization, i.e., after approximately 200,000 SPARK time iterations in the representative case shown in Fig. 8.

A. Injection and Energy Deposition

Drag and heat transfer reduction studies are first conducted using a forward-facing jet coupled with an energized region of the upstream flow to study the modification of the upstream flowfield around a hypersonic blunt body. For better understanding of the results obtained by combining these methods, the effectiveness of both injection alone and energy deposition alone, as well as the baseline (no flowfield modification), are discussed in this section.

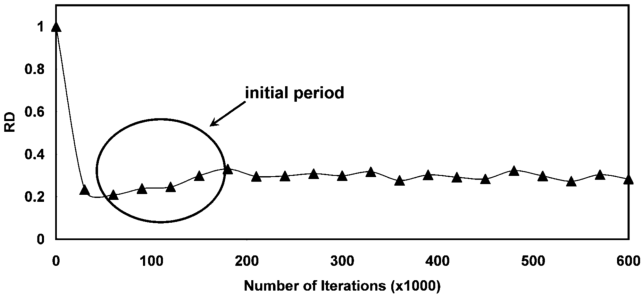

Fig. 8 Representative *RD* (drag reduction) vs iterations (time) showing initial jet penetration followed by partial collapse.

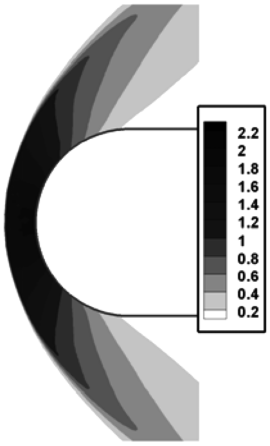

Fig. 9 Mach 10, baseline pressure-coefficient contours.

1. *Baseline*

The baseline (no flowfield modification) pressure contours for the nonadiabatic blunt body flow (body surface temperature of 500 K) at a flight Mach number of 10 are shown in Fig. 9. Note that all pressure contours in this work are nondimensionalized using the freestream dynamic pressure and static pressure (i.e., pressure contours are shown in terms of the pressure coefficient). From this figure, the nondimensional shock standoff distance for this case is $\Delta = 0.16$, where Δ is defined as the centerline distance from the leading edge of the blunt body to the blunt body shock front divided by the blunt body diameter. The baseline overall drag $D0$ and the baseline heat transfer rate $\dot{Q}$ are 1612 N and 9912 W, respectively. These values for the baseline case are very similar to results determined in other numerical studies and previously validated against experimental data (see [14]).

2. *Forward-Facing Injection Only*

Figure 10 depicts the pressure-coefficient contours generated for the case with a single-stream forward-facing jet. In this case, the injectant is N_2 with a nondimensional jet orifice diameter D/D_j of 63, injection total pressure P_{tj} of 375 kPa, and the injection Mach number M_j of 1.0. The forward-facing jet for all injection-alone cases (including the case shown) is highly unstable and generally simply "folded" back against the body with occasional limited excursions into the upstream. The "flapping" and unsettled behavior is typical of forward-facing jets in high-speed flows. Nevertheless, for completeness and comparisons, the time-averaged results for this case are given as follows: the nondimensional shock standoff

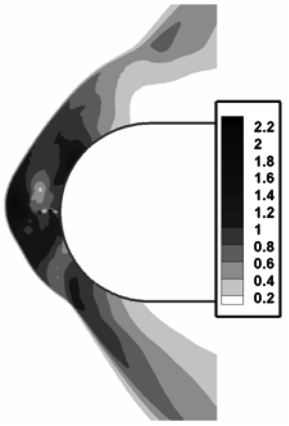

Fig. 10 Pressure coefficient contours, nitrogen injection without energy deposition.

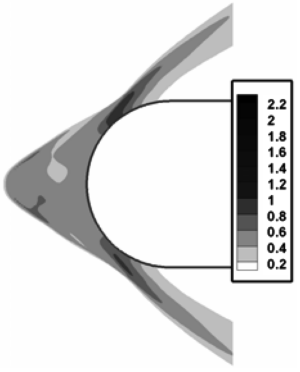

Fig. 11 Pressure coefficient contours, single energy deposition region without injection.

distance $\Delta = 0.23$, the drag reduction factor $RD = 0.92$, and the heat transfer reduction factor $RQ = 0.95$. This indicates an 8% reduction in overall drag and a 5% reduction in overall heat transfer due to the injection.

3. Energy Deposition Only

The pressure contours for a single energy deposition region upstream of the nonadiabatic blunt body (without injection) are shown in Fig. 11. In this case, a 30 kW energy rate is deposited in the upstream flow at a nondimensional location x/D of 1.5. The energy density is $1.5 \cdot 10^7$ kW/m^3 and has an energy deposition region aspect ratio a/b of 2.2. As measured from the pressure contours in Fig. 12, the nondimensional shock standoff distance is $\Delta = 0.48$. For this case, the drag reduction factor RD is 0.60, and the heat transfer reduction factor RQ is 1.1. This indicates a 40% drag reduction due to the energization coupled with a 10% increase in body heat transfer.

4. Forward-Facing Injection and Energy Deposition

The two techniques demonstrated previously (forward-facing injection and energy deposition) are now combined. Results are shown in Fig. 12, which is a plot of pressure contours for such a combination case. This plot is again for the nonadiabatic blunt body flow at the flight Mach number of 10 with a single forward-facing jet

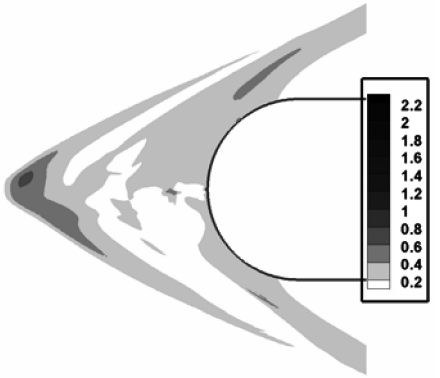

Fig. 12 Pressure coefficient contours, forward-facing injection with energy deposition.

and a single energy deposition region upstream. Here, the injectant is N_2 with a nondimensional jet diameter D/D_j of 63, a jet total pressure P_{tj} of 375 kPa, and the jet Mach number M_j of unity. Energy is deposited at a rate of 30 kW and is located at a nondimensional x/D of 1.5; energy density is $1.5 \cdot 10^7$ kW/m^3, and energy deposition aspect ratio a/b is 2.2. This case results in a nondimensional shock standoff distance Δ of 1.1, $RD = 0.34$, and $RQ = 0.37$.

Table 1 is a compilation of the data obtained in the previous (three) cases. The superiority of the forward-facing jet coupled with the energy deposition upstream of the blunt body is clearly seen by examining these results. The net effect of combining the two techniques is very significant in terms of greatly reduced drag and heat transfer as compared with the case with energy deposition alone. Furthermore, the effect on the jet is large: it penetrates far upstream and, as will be discussed in the next section, there is remarkable stabilization of the jet.

B. Effects of Chemical Reaction

This section examines the effect of energy deposition coupled with a forward-facing jet with and without chemical reaction for laminar flow conditions in the Mach 10 flight regime. The model that is used in this section uses an injectant core of H_2, which is sheathed or bordered above and below with N_2 injectant with the following injection conditions: a constant H_2 injectant jet Mach number M_{j,H_2} of 2.0, a constant nondimensional H_2 injectant jet diameter $D/D_{j,H_2}$ of 49, a constant N_2 injectant jet Mach number M_{j,N_2} of 1.0, and a combined constant nondimensional N_2 injectant jet diameter $D/D_{j,N_2}$ of 68. Also, as shown in Fig. 6, this model consists of three energy deposition regions with the following conditions: the centerline region A, at a nondimensional distance x/D of 1.5, has an energy rate of 90 kW, whereas the flank regions (B and C), each at nondimensional distances x/D (secondary) of 1.3 and $\pm y/D$ of 0.1, have a 50 kW energy rate deposition.

Figure 13 depicts the pressure contours generated for the case with forward-facing jets only with similar jet conditions described earlier. Here, the initialization flowfield for this case corresponded to the stabilized case of both injection and energy deposition (shown subsequently). As stated before, the forward-facing jet injection alone is highly unstable and generally, simply folded back against the body with occasional limited excursions into the upstream. Nevertheless, the time-averaged drag reduction factor RD is 0.95, indicating a 5% reduction in overall drag.

The pressure contours for three energy deposition regions upstream of the nonadiabatic blunt body (without injection) are

Table 1 Data summary of injection and energy deposition section

	Shock standoff distance, Δ	Drag reduction factor, RD	Heat transfer reduction factor, RQ
Baseline	0.16	1.00	1.00
Forward-facing jet	0.23	0.92	0.95
Energy deposition	0.48	0.60	1.10
Combined methods	1.10	0.34	0.37

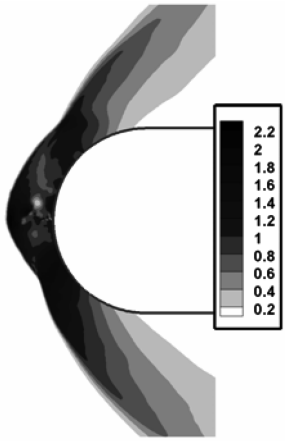

Fig. 13 Pressure coefficient contours, nitrogen and hydrogen injections without energy deposition.

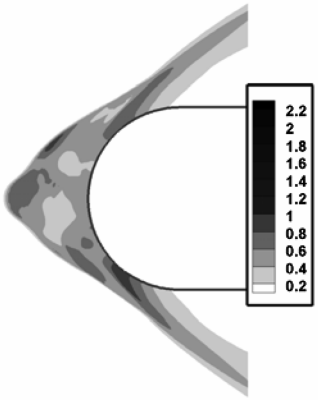

Fig. 14 Pressure coefficient contours, three energy deposition regions without injection.

shown in Fig. 14. The three energy deposition positions and conditions are described earlier. The actual energy deposition positions can be faintly observed in the following figure. For this case, the drag reduction factor *RD* is 0.54, indicating a 46% reduction in drag.

Figure 15 shows pressure and hydrogen mass fraction contours for the energy deposition coupled with forward-facing jets without chemical reaction (only mixing is allowed). This case served as the initialization flowfield for the other cases in this section. The forward-facing jets and the three energy deposition positions and conditions are similar to the ones which are described in the beginning of this section. After the flowfield reaches a quasi-steady state, the time-averaged drag reduction factor *RD* is 0.29, indicating a 71% reduction in overall drag.

The following study is conducted again using the same flowfield (mixing reaching its quasi-steady state) as the initial condition, and also used the hydrogen–air finite rate reaction, which used seven species and seven reactions. Figure 16 shows the pressure and reacted water mass fraction contours for this case. For this case, the time-averaged drag reduction factor *RD* is 0.29 and indicates a 71% drag reduction. Note that there is considerable water present in the shock layer and in the vicinity of the (flanking) energized zones. As was stated previously, chemical compositional changes (water production) due to the chemical reaction will enable efficient microwave or radiative heating.

Figure 17 plots the drag reduction factor *RD* vs the number of iterations for the earlier four studies conducted in this section. As can be seen, data are obtained at 30,000 iteration increments; the first 210,000 iterations represent the initial jet penetration and are not used in statistical bounds calculations. The use of the case with injection and energy deposition (no reaction) to provide the initialization flowfield for the other cases (at 600,000 iterations) is clearly indicated on this figure. The results demonstrate the superiority of the forward-facing jet coupled with the energy deposition upstream of the blunt body. Furthermore, although finite rate reaction has a very minimal effect on the time-averaged value of drag reduction factor *RD*, it seems to reduce the amount of fluctuation in the drag reduction, resulting in more stable forward-facing jets.

C. Effects of Energy Deposition and Injection on Jet Stability

As is seen in Fig. 17, stand-alone forward-facing injection in hypersonic/supersonic flow has major inherent limitations associated with the instability of the jet at most conditions as discussed in the Introduction section. This instability is manifested by jet plume fluctuations and results, in most cases, in the transient but complete collapse of the plume of the jet so that it variously bends and lies very close to the body before possibly partially recovering, etc. Consequently, upstream shock structures are highly transient and unsteady with resulting very large fluctuations in the values of drag *RD* and heat transfer reduction factors *RQ*. Because of the lack of effective jet penetration in stand-alone injection, the averaged drag and heat transfer reduction factors are close to unity.

In general, the coupling of the forward-facing injection with energy deposition as a means of drag and heat transfer reduction is shown here (see Fig. 17) to dramatically reduce these fluctuations and increase the stability of the forward-facing jet for all cases. The influence of reaction is minimal in either direction. The increase in stability by coupling energy deposition with the injection is generally found to result in a "bounded" stable jet throughout the stabilized time history (once the transients are finished) in terms of always eliminating the total collapse of the jet and usually ensuring far-forward and essentially stable penetration of the injectant. The zone that the forward-facing jet can oscillate in is apparently bounded by the oblique shock structure which is itself induced primarily by the energy deposition (and modified by the forward-facing injection itself).

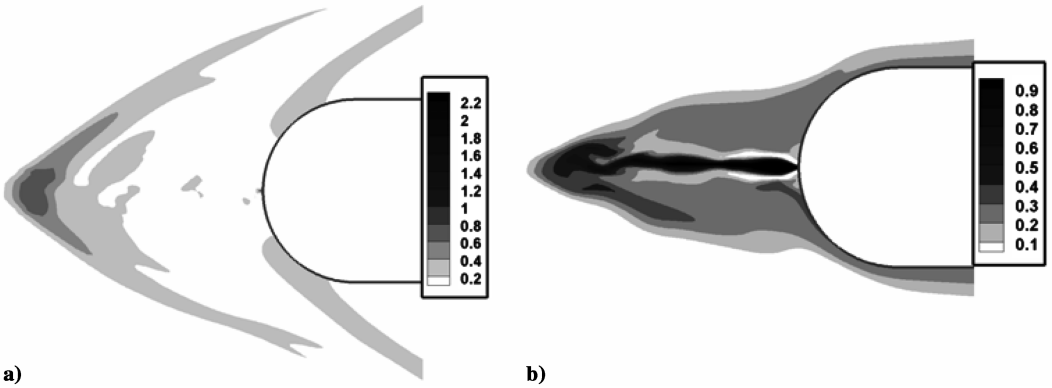

a) **b)**

Fig. 15 Injection and energy deposition, no reaction: a) pressure coefficient contours, b) hydrogen mass fraction contours.

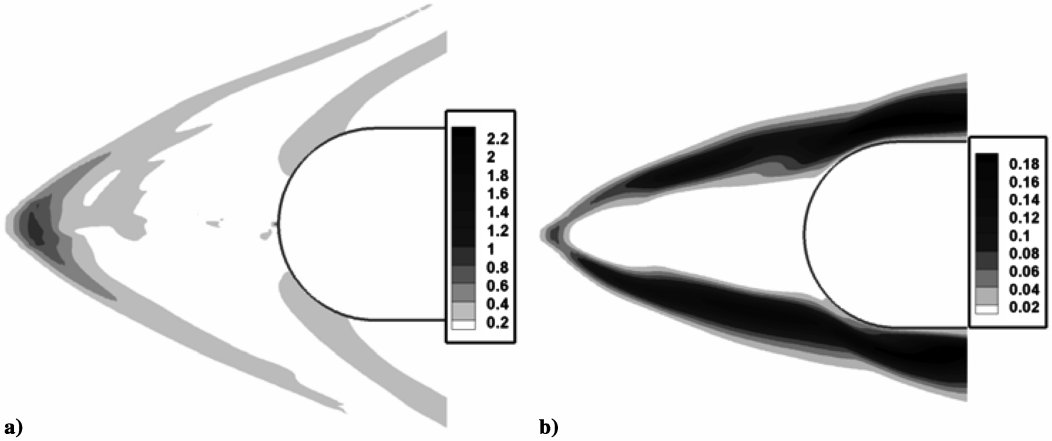

Fig. 16 Injection and energy deposition, with finite rate reaction: a) pressure coefficient contours, b) water mass fraction contours.

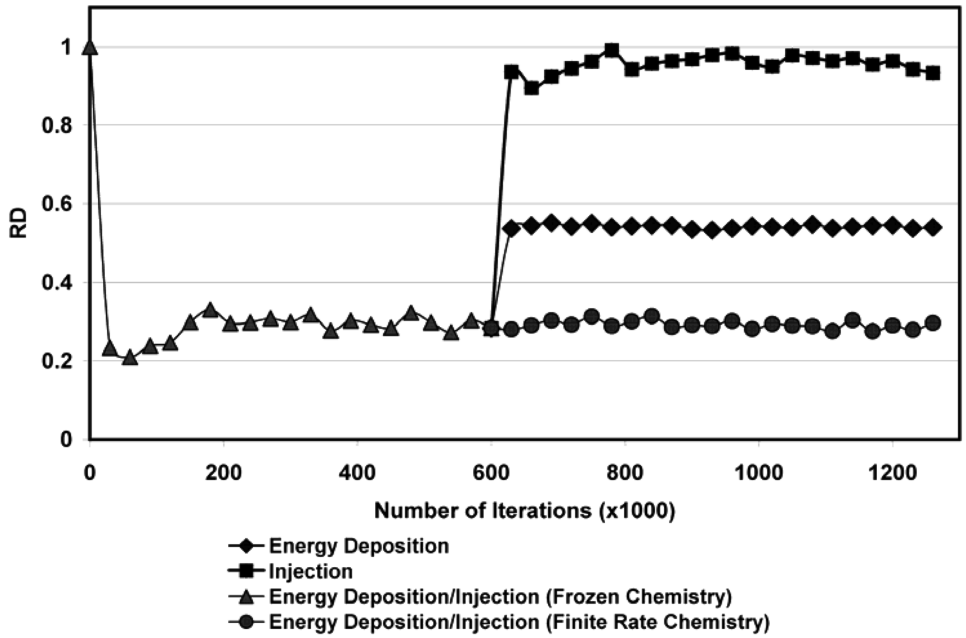

Fig. 17 *RD* (drag reduction factor) vs iteration (time) for varying conditions.

IV. VULCAN Study: Comparison of Laminar and Turbulent Injection/Energy Deposition

The remainder of the results reported on in this document used VULCAN to analyze the combined effects of upstream energy deposition and a forward-facing jet on the generic blunt body at flight Mach 10. The earlier SPARK studies focused entirely on the drag and heat transfer reduction *after* the flowfield had fully developed and then studied the bounded (transient or fluctuating) behavior within a selected interval to analyze jet stability [23]. The VULCAN studies, however, specifically and purposely looked at the (early) initial penetration of the jet into the flow as well as the transient response to (and beyond) jet stabilization thereafter. This could be done consistently because all the VULCAN cases were initialized from a common, converged baseline case. Because a statistical analysis regarding jet stability at "convergence" (i.e., bounded jet stabilization) was adequately conducted using SPARK (not shown in this paper, however, detailed in Khamooshi [23]), a more qualitative study focusing on the initial transients was conducted in the VULCAN cases. A major purpose for this was to study (and possibly control) the spatial placement or localization of H_2 (and reacted H_2O) with respect to energy deposition regions. This then mandates the visual examination of the initial penetration of the jet and the transient behavior of the flowfield to allow the (possible) development of control strategies to maintain H_2 (and hence reacted water) adjacent to the energy deposition regions. Here, both laminar and turbulent flowfields are shown to illustrate the impact of turbulence on flowfield behavior.

As a preliminary check, results generated by both SPARK and VULCAN were compared for a representative laminar case with energy deposition and injection. The flow features produced by the two codes were virtually identical with average drag reduction factors RD of 0.298 (SPARK) and 0.287 (VULCAN). The heat transfer was also examined for this (laminar) comparison case. The baseline heat transfer using SPARK was used to find the denominator of the heat transfer factor RQ for both SPARK and VULCAN results for the modified flow case compared. The resulting average heat transfer factors RQ are 0.874 (SPARK) and 0.888 (VULCAN).

A. VULCAN Case Studies

The VULCAN studies consisted of three energy regions in a configuration similar to that described in the sections of this paper which used the SPARK code. The centerline region A had an energy rate of 60 kW, whereas the flank regions (B and C) each had a 30 kW energy rate deposition. The aspect ratios of the three energy deposition regions were 0.8. The lead x/D was also 1.4 and the secondary x/D was 1.1. The flank regions also had a y/D of 0.1. All

injection studies used hydrogen sheathed by nitrogen jet. The total effective nitrogen D/D_j was 63 and the hydrogen D/D_j was 42. Both nitrogen and hydrogen were injected normal and at sonic velocity at 500 K and 50 kPa. The cases were conducted with 1) energy deposition alone, 2) energy deposition and injection (no reaction), and 3) energy deposition and H_2/N_2 injection with finite rate chemistry.

B. VULCAN Laminar and Turbulent Results

This section examines the coupled effect of energy deposition and a forward-facing jet on drag reduction for laminar and turbulent flow for the blunt body geometry using an adiabatic surface condition. As limiting cases, energy deposition without injection and injection without energy deposition are examined. The injection-only study found that the effect on drag reduction was minimal and thus will not be presented here. The laminar and turbulent results for the VULCAN results will be presented in the same order as were the earlier SPARK (laminar) results. The time history for laminar and turbulent cases was written out in 5 μs intervals. These intervals will also be referred to as "frames" in the following discussions.

1. *Energy Deposition Without Injection*

This subsection examines the effect of upstream energy addition on drag reduction without any injection from the blunt body. The small perturbations from the upstream energy deposition interact with the subsonic region upstream of the body and produce and then reinforce large recirculation zones in the shock layer which enlarge the subsonic region and cause the shock wave apex to penetrate further upstream toward the deposition region (i.e., the shock wave structure is more oblique). The weaker shock structure which results then produces a smaller pressure rise, which in turn decreases the drag on the body.

Pressure contours for energy deposition with no injection are shown in Fig. 18 for both laminar and turbulent flowfields. For this case without injection, the off-centerline (flank) deposition regions are placed too far from the centerline. As a consequence, the bow shock structure is blunted and is relatively close to the body with the side oblique shocks impinging on the body shoulders for both cases (laminar and turbulent). The *RD* is 0.69 and 0.66 for the laminar and turbulent cases, respectively, i.e., in this case the turbulent case demonstrates slightly better drag reduction.

2. *Energy Deposition with Injection (No Reaction)*

This subsection examines the effect of energy deposition coupled with a forward-facing jet without chemical reaction, i.e., only mixing is allowed. As modeled in earlier sections for laminar flow, the injectant core is H_2 which is sheathed or bordered above and below with N_2 injectant. The same injection conditions specified in earlier sections of this paper are used. As discussed earlier, the N_2 sheath has several advantages:

1) The N_2 will be relatively cool and will flow back and over the body thus shielding it from high temperature regions of the flow.

2) The N_2 has a relatively high molecular weight which will help to modify the shock structure upstream of the body.

3) The N_2 will insulate the injected hydrogen plume from the air adjacent to the nose until further upstream away from the body, such that reaction will be localized where water production is desired (i.e., as far upstream as possible near or in the energy deposition regions).

Studies of the time evolution of jets for a variety of initiating flowfield strategies and all cases examined in this work have shown that when injection and energy deposition are coupled, there is an initial period when the injection plume penetrates far upstream (corresponding to a maximum drag reduction, etc.) followed by a partial asymmetric collapse of the jet from that transient maximum penetration situation. The jet and shock structure (and associated drag and heat transfer reductions) then tend to stabilize within physical bounds as described in earlier sections (i.e., the solution exhibits bounded stability which has been of interest previously) but generally continue to oscillate. (Note that without energy deposition, the injection simply flaps back over the surface of the body with little or no penetration for almost all cases; a fact that has precluded much interest in the technique of forward-facing injection for any application.) It is of interest in this section to examine in more detail this transient behavior to (possibly) take advantage of techniques to increase penetration and hence drag reduction as well as to study the feasibility of localizing the hydrogen injectant in the vicinity of energy deposition.

Figure 19 shows results for the laminar flowfield with injection and heat deposition but without reaction at an initial time in the flowfield development. Although the jet does not penetrate all the way forward to the centerline energy deposition region (indeed it cannot because the centerline region is in supersonic flow), it does penetrate the gap between the flank (off-centerline) energy deposition regions and hence fills those regions with hydrogen. The injection plume does not partially collapse back (or "snap" back) as

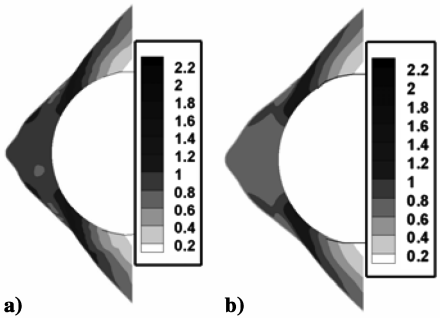

Fig. 18 Pressure coefficient contours in flowfield: energy deposition, no injection; a) laminar, b) turbulent.

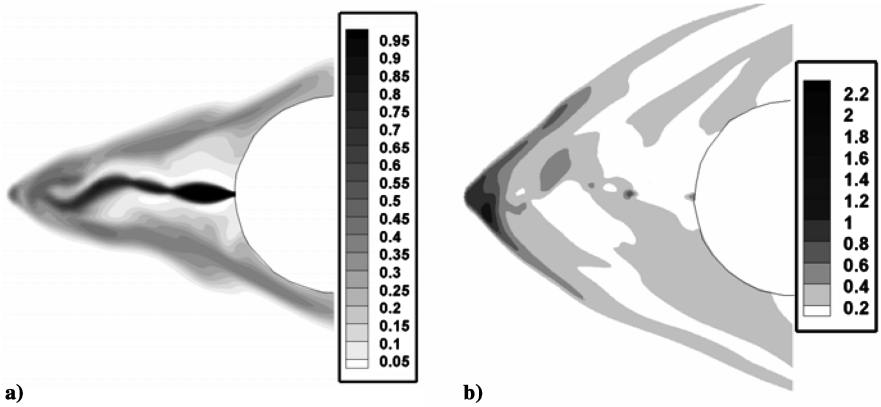

Fig. 19 Flowfield contours: energy deposition, injection, no reaction, initial time; laminar a) hydrogen mass fraction contours, b) pressure coefficient contours.

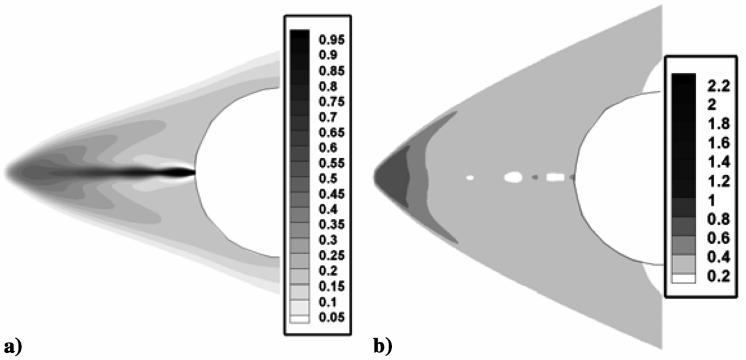

Fig. 20 Flowfield contours: energy deposition, injection, no reaction, initial time; turbulent a) hydrogen mass fraction contours, b) pressure coefficient contours.

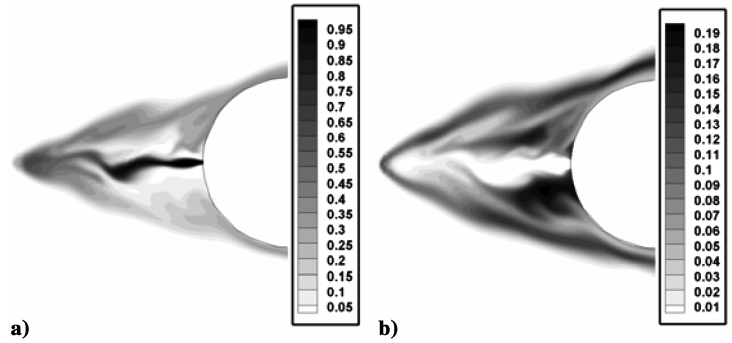

Fig. 21 Flowfield contours: laminar, finite rate reaction, initial time; a) hydrogen mass fraction contours, b) water mass fraction contours.

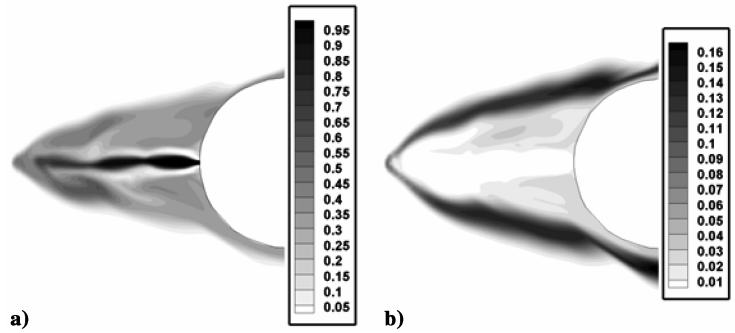

Fig. 22 Flowfield contours: laminar, finite rate reaction, later time; a) hydrogen mass fraction contours, b) water mass fraction contours.

discussed earlier but it nevertheless fluctuates or "flaps" in a limited sense. The *RD* for this case is around 0.32 after the initial small snap back.

Figure 20 shows the initial jet development for energy deposition, injection, no reaction case for the turbulent flowfield. The flow is more orderly and regular than observed for laminar flow. The same observations regarding the hydrogen "successfully" reaching the flank energized zones made for the laminar case earlier apply for the turbulent flowfield here. The jet subsequently partially collapses just as it does in the laminar solution but takes approximately twice as long to do so in real time. This suggests that the stability has been improved for the turbulent case. The *RD* before the partial collapse is approximately 0.25 and is approximately 0.33 after the partial collapse. Notice that the initial penetration is far enough that the flank energy regions are covered by a region of 50% hydrogen (by mass).

3. Energy Deposition/Injection with Finite Rate Chemistry

The following cases were conducted at the same conditions as for the previous case but with hydrogen–air finite rate reaction using 12 species and 24 reactions.

The hydrogen and water mass fraction contours shown in Fig. 21 are with finite rate reaction (laminar) and are at an early stage in the jet development. There are still relatively large water concentrations in the shocked layer from the initial mixing of the jet as it penetrates into the flowfield.

Figure 22 shows the flowfield contours for laminar conditions for this same case after about 40 frames. It can be seen that the majority of the initial water concentration has exited the domain. The nitrogen jet is sheathing the hydrogen and hence preventing it from reacting with the surrounding air (until the hydrogen has penetrated to the tip of the shock layer and mixed with the oxygen in the air). The jet is able to penetrate up to the energy addition regions and reacted water regions coincide with the flank energy deposition regions. This significantly helps the stability of the jet (preventing a partial collapse) in that it is still penetrating into the vicinity of the energy deposition locations after 40 frames with an *RD* of about 0.25. This *RD* well into the time evolution corresponds to the very early stages of the mixing case (but recall that quickly moved up to an *RD* of 0.32 due to injection plume partial collapse).

Figure 23 shows both hydrogen and water mass fraction contours with turbulence after approximately 40 frames. Note that there is still

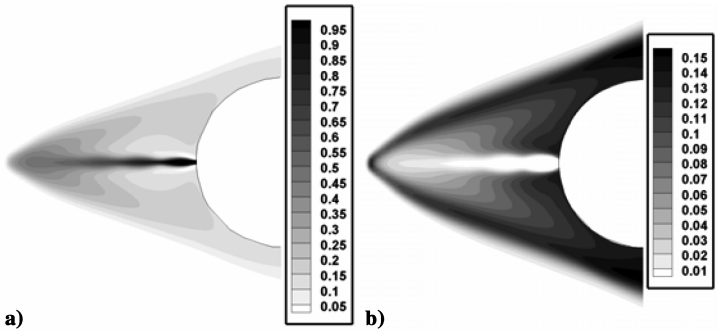

Fig. 23 Flowfield contours: turbulent, finite rate reaction; a) hydrogen mass fraction contours, b) water mass fraction contours.

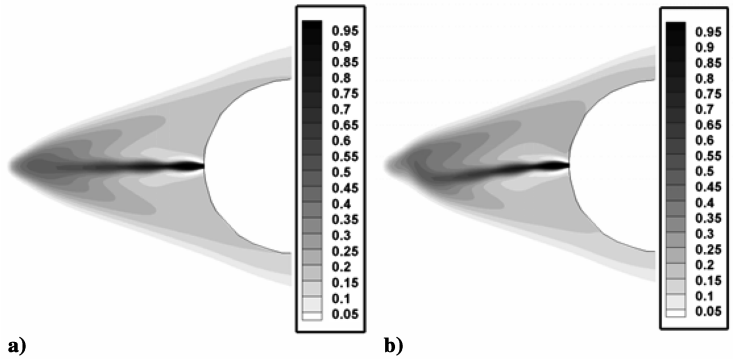

Fig. 24 Flowfield contours: turbulent, finite rate reaction, initial penetration and, a) beginning partial collapse, b) hydrogen mass fraction contours.

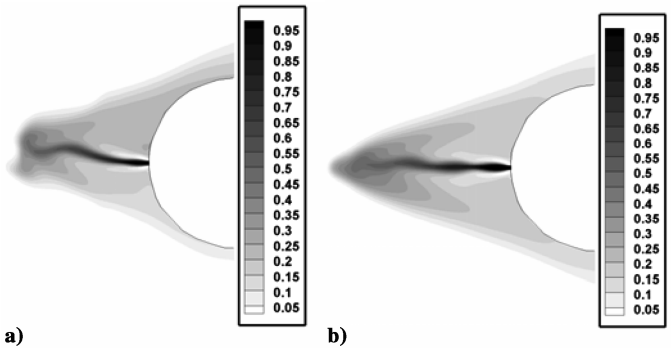

Fig. 25 Flowfield contours: turbulent, finite rate reaction, controlled recovery; hydrogen mass fraction contours.

considerable water present in the shock layer and in the vicinity of the (flanking) energized zones. This can be attributed to greater (turbulent) diffusion of the hydrogen into the air. The jet still behaves in the same manner as before with the same approximate *RD* of 0.25. It is, however, even more stable than exhibited in the laminar case. Even after 40 frames, there is little indication of any partial collapse.

V. Active Control of Jet Stability and Penetration

Because the turbulent cases with injection in the last section generally exhibited regular and "slow" partial collapse (considerably delayed from that of the laminar case), it is of interest to examine possibilities of controlling the flowfield (i.e., keeping far-forward jet penetration, etc.) by translating the energy deposition locations in a temporal schedule to keep the jet "stabilized." Figure 24 shows hydrogen contours at two times: 1) during initial penetration of the jet and 2) after the beginning of partial collapse, when the jet has begun to curve downward slightly. This configuration is for energy deposition, with injection, and finite rate reaction.

The entire set of three energy deposition region locations was then moved slightly off the centerline of the body (upward) and was kept there for three frames. Figure 25a shows the hydrogen contours at the end of this transient control process. The energy deposition locations were then moved back to their original (centered) locations and time advanced further. The contours in Fig. 25b show that the injection has recovered its approximate forward penetration condition.

Recall that the configuration without active control had resulted in the partial collapse of the jet (downward) with subsequent oscillations, but with slight pressurization on the upper side which tended to keep it curved somewhat down. With control of the energy deposition regions, when the energy deposition regions are appropriately moved away from the centerline as a partial collapse of the injection plume downward begins, a low-pressure wave travels downstream over the top surface of the jet thus causing it to curve back upward and recover maximum forward penetration (i.e., straighten). Conceptually, fast-acting pressure transducers on the blunt body could be used to determine when a jet was beginning a partial collapse and could then activate the translation of the energy deposition regions to restabilize the injection. This could (possibly) maintain drag and heat transfer reductions and water production in regions of energy deposition. It may be important to have an active control capability for such a system in general because the injection

will be susceptible to partial collapse due to small perturbations and nonuniformities in real systems. Further investigations need to be conducted to determine if a continually moving ("buzzing") energy deposition region could help to increase forward penetration and jet stability and hence minimize drag.

VI. Summary and Conclusions

This paper provides results from in-depth numerical studies of a two-dimensional blunt body at flight Mach 10. Of interest is the potential drag reduction obtained by coupling forward-facing fluid injection from the blunt body with upstream (localized) energy deposition. Heat transfer reduction, injection stabilization issues, and potential water production adjacent to upstream energized zones are also prominently discussed. It is found that the synergistic combination of these two effects (energy deposition and forward-facing injection) always provides for a significant reduction in overall drag on the representative blunt body examined. Furthermore, and of critical importance, the combination of the two methods provides for a substantial increase in the stability of the forward-facing injection, i.e., the combination dramatically increases and stabilizes forward penetration of injectant and prevents the total collapse of the injection plume.

For laminar flow calculations, the drag reduction with injection alone (for representative cases) is only approximately 5% from the baseline (blunt body with no flowfield modification) case. This is primarily due to the (expected) complete collapse of the injectant plume. For the laminar case with energy deposition by itself (no injection), resultant drag is approximately 55% of the baseline. However, when the two techniques are combined (laminar flow), the drag is approximately 28% of the baseline and stabilized forward penetration of the jet (within bounds) is observed. Furthermore, by sheathing the core hydrogen injectant with a cool inert gas (nitrogen in this study), the heat transfer to the body was simultaneously and significantly reduced.

For laminar flow (Navier–Stokes) calculations, when nitrogen alone is injected (no hydrogen), two major physical parameters are found to drive drag reduction:

1) Lower injection Mach number reduces the drag and heat transfer regardless of energy deposition location.

2) Larger energy deposition aspect ratio a/b also decreases drag. When a hydrogen core is injected with nitrogen sheathing, maximum effectiveness in terms of penetration of hydrogen plume upstream was found by defining a three-zone region of energy deposition composed of a centerline upstream zone and flanked by two (off-centerline) energized zones slightly downstream. This tended to allow the penetration of the injectant between the two flanking energy zones. When reaction is allowed, substantial water production in the vicinity of the two flanking energy zones is observed which may allow more efficient energy deposition techniques (such as microwaves). In addition, the impact of reaction (heat release due to chemical kinetics) tended to increase jet stabilization.

The impact of turbulence on drag reduction and flow stability (for combined energy deposition and forward-facing injection) was also studied. Also, the transient behavior of the initial jet and flowfield was examined in detail. This was of interest because it was observed in the course of the study that maximum forward penetration of the jet and lowest drags were obtained in the transient phase, when the jet is initially penetrating and the flowfield is evolving. The impact of turbulence on drag reduction results was found to be minimal, i.e., the RD (drag reduction factor) is not appreciably affected by turbulence. Turbulence also generally increased the stability of the forward-facing injection, delaying the partial collapse, and increased mixing of hydrogen and air. This increased mixing results in more effective energy release associated with reaction which is found to further stabilize the injection and results in lower drag. The localization of reacted water production in the vicinity of the upstream energized zones is shown to be practical and may result in a more efficient energy deposition technique for transmission of some of the energy upstream into the flow. Finally, the conceptual use of an active control system resulting in a translating (moving) energy deposition region(s) is shown to allow the control of the jet to effect maximum penetration and minimum drag.

Acknowledgments

The authors gratefully acknowledge the support and advice of Charles McClinton and Aaron Auslender of the NASA Langley Research Center in the course of this work. Financial support for this work was received through NASA NAG1-01122 and NASA NGT1-03011 (Graduate Student Researchers Program Training Grant).

References

[1] Knight, D., "Survey of Aerodynamic Flow Control at High Speed by Energy Deposition," AIAA Paper No. 2003-0525, Jan. 2003.

[2] Marconi, F., "An Investigation of Tailored Upstream Heating for Sonic Boom and Drag Reduction," AIAA Paper 98-0333, Jan. 1998.

[3] Riggins, D. W., Nelson, H. F., and Johnson, E., "Blunt Body Wave Drag Reduction Using Focused Energy Deposition," *AIAA Journal*, Vol. 37, No. 4, 1999, pp. 460–467.

[4] Kogan, M., Ivanov, D., Shapiro, E., and Yegorov, I., "Local Heat Supply Influence on a Flow over a Sphere," AIAA Paper 2000-0209, Jan. 2000.

[5] Taylor, T., "Drag Reduction and Control Using Energetics and Electrostatic Force-Fields for Hypersonic Applications," AIAA Paper 2004-0131, Jan. 2004.

[6] Taylor, T., "Numerical Investigation of Potential Flow-Field Modification Techniques: Drag Reduction, Control, And Enhanced Fuel-Air Mixing in Hypersonic Vehicles," Master's Thesis, Mechanical and Aerospace Engineering Dept., Univ. of Missouri, Rolla, MO, 2004.

[7] Riggins, D. W., Barnett, J. T., and Taylor, T., "Drag Reduction and Heat Transfer Mitigation for Blunt Bodies in Hypersonic Flight: A Survey of Techniques," AIAA Paper 2003-6968, 2003.

[8] Froning, H. D., and Roach, R. L., "Application of CFD to Problem of Drag Reduction by Free Stream Perturbations," AIAA Paper 98-2655, June 1988.

[9] Hutt, G. R., and Howe, A. J., "Forward Facing Spike Effects on Bodies of Different Cross Section in Supersonic Flow," *Journal of the Royal Aeronautical Society*, Vol. 93, No. 6, 1989, pp. 229–234.

[10] Yamauchi, M., Fujii, K., and Higashino, F., "Numerical Investigation of Supersonic Flows Around a Spiked Blunt Body," *Journal of Spacecraft and Rockets*, Vol. 32, No. 1, 1995, pp. 32–42.

[11] Mehta, R. C., "Numerical Heat Transfer Study Over Spiked-Blunt Body at Mach 6.8," AIAA Paper 2000-0344, Jan. 2000.

[12] Barnett, J. T., "Numerical Investigation of the Impact of Hypersonic Shadowing on Drag and Heat Transfer for a Blunt Body," Master's Thesis, Mechanical and Aerospace Engineering Dept., Univ. of Missouri, Rolla, MO, 2004.

[13] Charczenko, N., and Hennessey, K. W., "Investigation of a Retrorocket Exhausting from the Nose of a Blunt Body into a Supersonic Free Stream," NASA TN D-751, Sept. 1961.

[14] Meyer, B., "Numerical Investigation of Hypersonic Drag and Heat Transfer Using a Forward-Facing Jet," Master's Thesis, Mechanical and Aerospace Engineering Dept., University of Missouri, Rolla, MO, 2000.

[15] Meyer, B., Nelson, H. F., and Riggins, D. W., "Hypersonic Drag and Heat Transfer Reduction Using a Forward Facing Jet," *Journal of Aircraft*, Vol. 38, No. 4, 2001, pp. 680–686.

[16] Charwat, A. F., "Investigation of the Flow and Drag Due to Supersonic Jets Discharging Upstream into a Supersonic Flow," NASA TR AD-603354, July 1964.

[17] Love, E. S., "The Effects of a Small Jet of Air Exhausting From the Nose of a Body of Revolution in Supersonic Flow," NACA RM L52I19a, Nov. 1952.

[18] Romeo, D. J., and Sterrett, J. R., "Exploratory Investigation of the Effect of a Forward-Facing Jet on the Bow Shock of a Blunt Body in Mach 6 Free Stream," NASA TN D-1605, Feb. 1963.

[19] Tolle, F. F., "An Investigation of the Influence of a Forward Ejected Gas Stream on Hypersonic Flow about Blunt Bodies," Ph.D. Dissertation, Mechanical and Aerospace Engineering Dept., Univ. of Arizona, Tucson, AZ, 1973.

[20] Finley, J. P., "The Flow of a Jet from a Body Opposing a Supersonic Free Stream," *Journal of Fluid Mechanics*, Vol. 26, Pt. 2, Oct. 1966, pp. 337–368.

[21] Drummond, J. P., Rogers, R. C., and Hussaini, M. Y., "A Detailed Numerical Model of a Supersonic Reacting Mixing Layer," AIAA

Paper 86-1427, June 1986.
[22] Viscous Upwind Algorithm for Complex Flow Analysis (VULCAN) User Manual, Ver. 6.0.0, NASA Langley Research Center, Hampton, VA, 2007, http://vulcan-cfd.larc.nasa.gov/.
[23] Khamooshi, A., "Numerical Investigation of the Effects of Coupling Upstream Energy Deposition and Forward-Facing Injection on a Blunt Body in Mach 10 Flight," Master's Thesis, Mechanical and Aerospace Engineering Dept., Univ. of Missouri, Rolla, MO, 2005.

N. Clemens
Associate Editor